Threshold Collision-Induced Dissociation of Hydrogen-Bonded Dimers of Carboxylic Acids

Beike Jia,[†] Laurence A. Angel,[‡] and Kent M. Ervin*

Department of Chemistry and Chemical Physics Program, University of Nevada, Reno, 1664 North Virginia Street MS 216, Reno, Nevada 89557-0216

Received: December 3, 2007

Energy-resolved competitive collision-induced dissociation is used to investigate the proton-bound heterodimer anions of a series of carboxylic acids (formic, acetic, and benzoic acid) and nitrous acid with their conjugate bases. The dissociation reactions of the complexes $[CH_3COO{\cdot}H{\cdot}OOCH]^-$, $[CH_3COO{\cdot}H{\cdot}ONO]^-$, $[HCOO{\cdot}H{\cdot}ONO]^-$, $[C_6H_5COO{\cdot}H{\cdot}OOCH]^-$, and $[C_6H_5COO{\cdot}H{\cdot}ONO]^-$ are investigated using a guided ion beam tandem mass spectrometer. Cross sections of the two dissociation channels are measured as a function of the collision energy between the complex ions and xenon target gas. Apparent relative gas-phase acidities are found by modeling the cross sections near the dissociation thresholds using statistical rate theory. Internal inconsistencies are found in the resulting relative acidities. These deviations apparently result from the formation of higher-energy conformers of the acids within the complex ions induced by double hydrogen bonding, which impedes the kinetics of dissociation to ground-state product acid conformations.

Introduction

Competitive threshold collision-induced dissociation (TCID)[1,2] has been shown to be a powerful method for measuring the relative gas-phase acidity between an unknown acid (HA_2) and a reference acid (HA_1).[2−4] The first step is to form a proton bound complex $[A_1HA_2]^-$ by combining A_1^- with HA_2 or A_2^- with HA_1. The complex then collides with Xe at a controlled translational energy, and dissociates into two product channels, eq 1.

$$[A_1HA_2]^- + Xe \rightarrow HA_1 + A_2^- + Xe \quad (1a)$$

$$\rightarrow HA_2 + A_1^- + Xe \quad (1b)$$

If there are no reverse activation barriers for these two channels, then the relative acidities are given by eq 2, where E_0(1a) and E_0(1b) are the reaction thresholds for (1a) and (1b),

$$\Delta E_0 = E_0(1a) - E_0(1b) = \Delta_{acid}H_0(HA_2) - \Delta_{acid}H_0(HA_1) \quad (2)$$

respectively, and $\Delta_{acid}H$ is the enthalpy change of the deprotonation reaction $HA \rightarrow H^+ + A^-$. If the gas-phase acidity for one of the acids is known and the threshold difference ΔE_0 is measured, then the acidity of the other acid may be found from eq 2. The two reaction thresholds, E_0(1b) and E_0(1a), along with the energy dependent branching ratio are modeled by statistical rate theory to fit the TCID cross sections.[1,2,5] In our laboratory, the relative acidities of a series of alcohol molecules, where the proton in the complex is shared by two oxygen atoms, have been measured[2,4] and shown to provide accurate results.[6]

This work investigates the application of the TCID method to formic, acetic, and benzoic acids with nitrous acid as a reference. These systems present an additional challenge for TCID because the hydrogen binding interactions at the two oxygen atoms in a carboxylic acid molecule and formation of various conformers may complicate the kinetics of dissociation. We examine how these factors affect the TCID process.

Experimental Methods

The details of the competitive TCID experiments and the guided ion beam tandem mass spectrometer have been described previously.[2,4,7] A_1^- anions are generated in a flow tube reactor (FTR) by introducing an adjustable flow of a precursor gas to a microwave discharge source. The HA_2 acids (HCOOH, CH_3COOH, or C_6H_5COOH) are added downstream to form $[A_1HA_2]^-$ complexes by addition to A_1^- ($HCOO^-$, CH_3COO^-, or NO_2^-). Collisions with the He buffer gas in the FTR at a pressure of about 0.5 mbar serve to thermalize the ions. $HCOO^-$ and CH_3COO^- are produced from the formic and acetic acid vapors. Although gaseous HNO_2 is not readily available,[8] NO_2^- anions are easily produced from air in the microwave discharge. Therefore, all the complexes containing NO_2^- are created from the combination of NO_2^- with HA_2. Negative ions are sampled from the FTR through a 1-mm-diameter aperture in a conical nose cone and then extracted, accelerated and focused by a series of electrostatic lenses before entering a magnetic sector where the $[A_1HA_2]^-$ complex is selected by mass. The $[A_1HA_2]^-$ anions are then decelerated, focused and injected by another series of lenses into an octopole ion beam guide where the ions are trapped radially by a radio frequency field.[9] The axial kinetic energy of the ion beam is controlled by a dc potential applied on the octopole rods. To determine the kinetic energies of the beam, a retarding potential analysis is used by scanning the dc component on the octopole and measuring the resulting ion beam intensity.[10] A time-of-flight (TOF) measurement is also employed periodically to check the results from retarding potential analysis.[7] A 7.0 cm long gas cell in which the collision-induced dissociation occurs is mounted along the octopole for introduction of Xe target gas. The gas pressure in the gas cell is measured by an ionization gauge on the octopole chamber calibrated at higher pressures to a capacitance manometer connected to the gas cell. The product ions, A_1^- and A_2^-, and the nondissociated

* Corresponding author. Electronic mail: ervin@unr.edu.
[†] Current address: SRI International, Menlo Park, CA.
[‡] Current address: Department of Chemistry, Texas A&M University at Commerce.

10.1021/jp7114093 CCC: $40.75
Published on Web 01/31/2008

$[A_1HA_2]^-$ complex ions continue to travel in the octopole field beyond the gas cell until they arrive at the extraction focusing stage and are then mass analyzed by a quadrupole mass spectrometer. To achieve better mass abundance sensitivity for NO_2^- (46 amu) and $HCOO^-$ (45 amu), the second stability region of the Mathieu stability diagram is employed,[7] whereas usually the first stability region is used for other experiments. The ion intensities are counted by a collision dynode/channeltron multiplier operated in negative ion counting mode.

The translational energy of the ion beam is scanned from near zero energy up to a few electron volts. These energies are then converted to the relative collision energies in the center-of-mass frame using the masses of the collision pair under the stationary target approximation.[10] Three different Xe gas pressures are used for each dissociation process and the apparent reaction cross sections are determined by Beer's law.[7,10] The reaction cross sections in the single-collision limit are obtained by extrapolating the apparent cross sections to zero pressure. The absolute cross section magnitudes have an uncertainty of about ±50%, but the two product channels' relative values are within ±10%.

Competitive TCID Cross Section Analysis. After the collision with Xe gas, the complex $[A_1HA_2]^-$ becomes an energized molecule and its internal energy, $E^* = E_i + \epsilon$, will then include the initial thermal internal energy E_i from the ion source (calculated as a Boltzmann distribution) plus the energy ϵ acquired from the collision with Xe gas. The latter is modeled with the empirical energy-transfer distribution function given by eq 3,[11] where E is the relative collision energy, σ_0 is a scaling

$$P_e(\epsilon,E) = \sigma_0 N \frac{(E-\epsilon)^{N-1}}{E} \tag{3}$$

factor related to the total collision cross section, and N is an adjustable parameter that describes the efficiency of translational to internal energy transfer. The probability of dissociation of the energized complex into channel j ($j = 1$ or 2) is given by first-order reaction kinetics with parallel product channels resulting in eq 4, where k_j is the dissociation rate constant from

$$P_{D,j}(E^*,\tau) = \frac{k_j(E^*)}{\sum k_j(E^*)}[1 - \exp(-\sum k_j(E^*)\tau)] \tag{4}$$

Rice-Ramsperger-Kassel-Marcus (RRKM) statistical rate theory for product channel j and τ is the experimental time window for dissociation to occur between the gas cell and the detector. The expression for the RRKM rate constants[12,13] is given by eq 5, where $N^{\ddagger}_{vr,j}$ is the sum of active ro-vibrational states at the

$$k_j(E^*,J) = \frac{s_j N^{\ddagger}_{vr,j}(E^* - E_0(j))}{h\rho_{vr}(E^*)} \tag{5}$$

transition-state configuration, ρ_{vr} is the density of states of the energized molecule, h is Planck's constant, and s_j is the reaction degeneracy. More complete forms of eqs 4 and 5 including angular momentum effects are actually used and have been presented previously.[1,2,5] The ro-vibrational densities of states for the RRKM calculations and the internal energy distribution are calculated using the Beyer−Swinehart Stein-Rabinovitch algorithm.[14−16]

The transition states (TS) in the RRKM theory may be treated as fixed (tight), orbiting (loose, i.e., located at the centrifugal barrier), or with a transition-state-switching model.[12,13,17] For a loose, orbiting TS there is no potential energy barrier along the reaction coordinate, which is appropriate for the dissociation of many electrostatically bound ion−molecule complexes. This model is usually valid for proton-bound dimer anion complexes because they are held together by ion−induced-dipole attraction and hydrogen-bonding rather than by covalent bonds. The orbiting TS at the centrifugal effective potential barrier has the same vibrational frequencies as the free fragments because it occurs at a relatively large separation of the products, whereas the intermolecular modes are treated as free rotors. The centrifugal barrier is calculated using the locked-dipole approximation.[4] The transition-state-switching model uses a loose orbiting TS at large distance between the fragments and a fixed tight TS at small distance.[17] For the TS switching model, the sum of states in the numerator of eq 5 is replaced by the smaller of the values calculated for the tight and loose transition states, evaluated at each total energy and angular momentum.

The rotational constants and vibrational frequencies for the complexes and products used in this work are either experimental values from the literature or computed values at the B3LYP/aug-cc-pVDZ level with Gaussian 03.[18−20] Table S1 in the Supporting Information lists the adopted values. The vibrations are treated in the independent-oscillator harmonic-oscillator approximation, except that the methyl rotors in carboxylic acid and carboxylate and the phenyl rotors in benzoic acid and benzoate are treated as free or hindered rotors[2] with parameters given in Table S1. The model cross sections are further convoluted with experimental energy distributions[10,21] and fit to the two reaction channel cross sections simultaneously with nonlinear least-squares optimization to obtain $E_0(1)$, ΔE_0, σ_0, N, and where noted an adjustable scaling factor for the second product channel,[1] which has the effect of adjusting the relative sum of states in eq 5. These calculations and fits are performed using the CRUNCH Fortran program.[22] Further details of the cross section modeling, including convolutions over translational and internal energy distributions and the treatment of rotational distributions in the RRKM rate theory calculations, may be found in previous work.[1−4,10]

Experimental Results

The single-collision cross sections and fits for the dissociation reactions are shown in Figure 1. The solid lines going through the experimental points are fits convoluted with the energy distributions whereas the dashed lines are the 0 K unconvoluted model cross sections. We first assume a simple approach and consider a single conformation of the cluster ion that can dissociate to two pairs of products in their ground-state conformations. These fits (model A) are shown in the left column of Figure 1 and the parameters are given in Table 2. Model A uses loose transition states for both product channels, as usually appropriate for dissociation of proton-bound cluster ions. We found acceptable fits for $[CH_3COO{\cdot}H{\cdot}OOCH]^-$ and $[CH_3COO{\cdot}H{\cdot}ONO]^-$, but the fits for $[HCOO{\cdot}H{\cdot}ONO]^-$, $[C_6H_5COO{\cdot}H{\cdot}OOCH]^-$, and $[C_6H_5COO{\cdot}H{\cdot}ONO]^-$ are marginal. In particular, the higher-energy channels of these systems could be fit only over a restricted energy range near threshold.

For all five systems, improved fits including the plateau region could be obtained if one product channel was allowed to have a relative scaling factor different unity. These fits (model B) are shown in the right column of Figure 1 and the parameters are given in Table 2. Similar fits (not shown) can be obtained by treating the higher energy channel with the transition-state-switching model with the relative energy of the of the inner, tight transition state treated as an adjustable parameter (instead of the scaling factor). Either method adds an adjustable

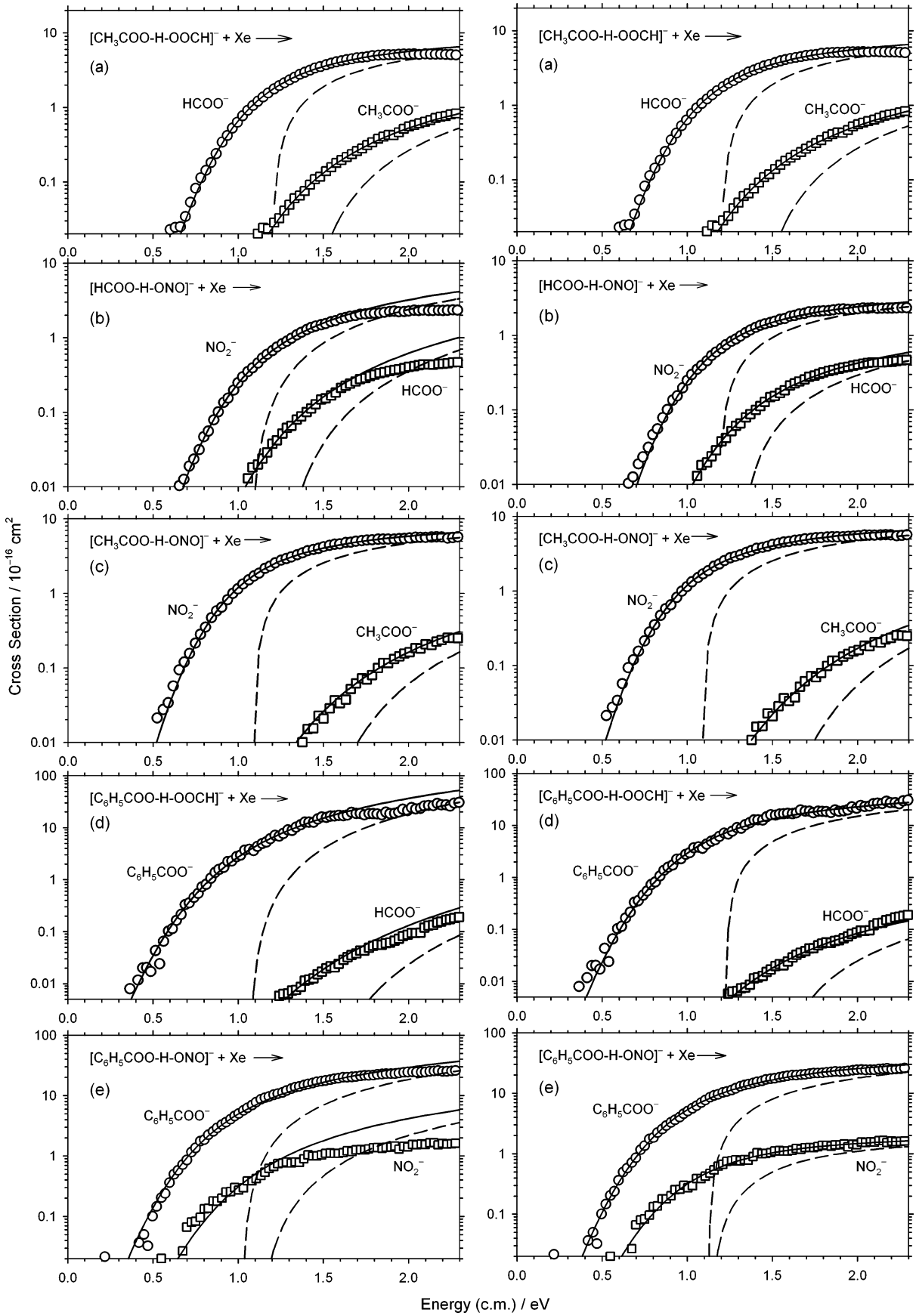

Figure 1. Energy-resolved threshold collision-induced dissociation cross sections for (a) $[CH_3COO{\cdot}H{\cdot}OOCH]^- \rightarrow HCOO^- + CH_3COOH$ (circles), $HCOOH + CH_3COO^-$ (squares); (b) $[HCOO{\cdot}H{\cdot}ONO]^- \rightarrow NO_2^- + HCOOH$, $HNO_2 + HCOO^-$ (squares); (c) $[CH_3COO{\cdot}H{\cdot}ONO]^- \rightarrow NO_2^- + CH_3COOH$ (circles), $CH_3COO^- + HNO_2$ (squares); (d) $[C_6H_5COO{\cdot}H{\cdot}OOCH]^- \rightarrow C_6H_5COO^- + HCOOH$ (circles), $C_6H_5COOH + HCOO^-$ (squares); (e) $[C_6H_5COO{\cdot}H{\cdot}ONO]^- \rightarrow C_6H_5COO^- + HNO_2$ (circles), $+ NO_2^- + C_6H_5COOH$ (squares). The data are the same in both columns; the left column shows the fits using model A and the right column shows the fits using model B, described in the text. The solid lines are the fits to the data; the dashed lines are the corresponding model cross sections at 0 K without energy convolutions.

TABLE 1: TCID Cross Section Fits with RRKM Models

Model A. No scaling

acid pair[a]	σ_0	N	E_0 (1)	ΔE_0	n
(1) CH_3COOH, HCOOH	14.2	1.22	1.19 ± 0.09	0.143 ± 0.041	6
(2) HCOOH, HNO_2	10.1	1.72	1.10 ± 0.20	0.115 ± 0.046	4
(3) CH_3COOH, HNO_2	17.9	1.14	1.09 ± 0.10	0.272 ± 0.049	3
(4) HCOOH, C_6H_5COOH	53.8	1.87	1.12 ± 0.21	0.269 ± 0.044	4
(5) HNO_2, C_6H_5COOH	41.1	2.05	1.0 ± 0.4	0.061 ± 0.024	3

Model B. Higher-Energy Product Channel with Independent Adjustable Scaling Factor $S_0(2)$

	σ_0	N	E_0 (1)	ΔE_0	$S_0(2)$	n
(1) CH_3COOH, HCOOH	14.1	1.20	1.18 ± 0.08	0.183 ± 0.087	2.8	6
(2) HCOOH, HNO_2	8.4	1.09	1.21 ± 0.12	0.084 ± 0.067	0.47	4
(3) CH_3COOH, HNO_2	17.9	1.15	1.09 ± 0.10	0.28 ± 0.13	1.27	3
(4) HCOOH, C_6H_5COOH	51.9	1.33	1.20 ± 0.17	0.230 ± 0.086	0.26	4
(5) HNO_2, C_6H_5COOH	39.8	1.47	1.06 ± 0.17	0.002 ± 0.030	0.062	3

Model C. Including Conformers of Complex and Products as Statistically Accessible

	σ_0	N	E_0 (1)	ΔE_0	n
(1) CH_3COOH, HCOOH	14.2	1.18	1.19 ± 0.09	0.145 ± 0.041	6
(2) HCOOH, HNO_2	10.3	1.72	1.10 ± 0.20	0.132 ± 0.046	4
(3) CH_3COOH, HNO_2	17.9	1.15	1.10 ± 0.10	0.303 ± 0.049	3
(4) HCOOH, C_6H_5COOH	53.9	1.86	1.12 ± 0.21	0.268 ± 0.044	4
(5) HNO_2, C_6H_5COOH	40.0	1.90	1.0 ± 0.5	0.051 ± 0.024	3

[a] Species with smaller value of $\Delta_{acid}H_0$ listed first.

TABLE 2: Gas-Phase Acidities (kJ/mol)

	CH_3COOH	HCOOH	C_6H_5COOH	HNO_2	χ_{acid}^2
$\Delta_{acid}H_0$, TCID model A	1446 ± 4	1433 ± 7	1411 ± 7	1418.5 ± 0.9 (ref)[a]	5.8
$\Delta_{acid}H_0$, TCID model B	1448 ± 7	1431 ± 12	1417 ± 9	1418.5 ± 0.9 (ref)[a]	12.5
$\Delta_{acid}H_0$, TCID model C[b]	1448 ± 4	1435 ± 6	1412 ± 6	1418.5 ± 0.9 (ref)[a]	4.8
$\Delta_{acid}H_0$, G3[c]	1450.1	1435.0	1418.2	1416.9	
$\Delta_{acid}H_0$, CBS-QB3[d]	1447.5	1432.0	1414.4	1415.0	
$\Delta_{acid}H_0$, CCSD(T)[e]	1450.3	1435.1	1418.4	1420.7	
$\Delta_{acid}G_{298}$, NIST[f]	1427 ± 8	1415 ± 8	1393 ± 8		
$\Delta_{acid}H_{298}$, NIST[g]	1453 ± 10	1444 ± 10	1422 ± 11		
$\Delta_{acid}H_0$, NIST[g]	1447 ± 12	1439 ± 12	1416 ± 13		

[a] Fixed reference acidity from $\Delta_{acid}H_0(HNO_2) = D_0(H-ONO) + IE_0(H) - EA_0(NO_2)$, with $D_0(H-ONO) = 325.8 \pm 0.8$ kJ mol^{-1};[26] $IE_0(H) = 1312.0496 \pm 0.0010$ kJ mol kJ^{-1};[26] and $EA_0(NO_2) = 219.3 \pm 0.5$ kJ mol^{-1}.[27] [b] Recommended TCID values. [c] Gaussian-3 method.[29] [d] Complete basis set method.[30] [e] CCSD(T)/aug-cc-pVTZ//B3LYP/aug-cc-pVTZ with vibrational zero-point energy corrections at the B3LYP/aug-cc-pVTZ level. [f] Equilibrium acidity values[33−35] from the NIST compilation.[32] [g] Converted from the NIST Gibbs energy using molecular constants in Table S1.

parameter for one channel, which naturally improves the fits to the data and allows fitting over a wider energy range from threshold up to the plateau of the cross sections. As an extreme example, the sum of squared residuals for fitting the $[C_6H_5COO{\cdot}H{\cdot}ONO]^-$ dissociation cross sections is over 6 times smaller using the extra scaling factor. Separate adjustable parameters for the two channels in competitive TCID have been used previously[1,23,24] and can in principle be rationalized (1) to account for the possible experimental mass discrimination errors; (2) for the case that the transition state of one channel is "tighter" than the other because of features of the potential energy surface along the dissociation path; or (3) to compensate for possible deficiencies in the ro-vibrational density of states calculation that affects one channel differently than the other. Case (3) could be operative if, for example, the actual rotational symmetries at the centrifugal barrier of the loose transition state are lower than those of the free products as assumed.

The errors for individual ΔE_0 values listed in Table 1 are estimates of ±2 standard uncertainties.[25] The uncertainty limits include the statistical deviation of data taken on separate occasions; the ion beam energy zero uncertainty (±0.05 eV laboratory); the consistency of the model fit over different energy ranges; statistical errors from the least-squares procedure estimated by changing ΔE_0 to produce a factor of 2 increase in the sum-of-squared-residuals; and the RRKM model uncertainty estimated by varying the scaling factor of one channel relative to the other by factors of 0.5 and 2.0 (equivalent to changes in the sum of states, reaction degeneracy, or rate constant by the same factors) and re-optimizing other parameters. Although the fits to the data are better over a wider energy range using the independent scaling factor for one channel in model B, the uncertainties in the ΔE_0 values are larger than for model A without scaling. That results from a strong correlation between the scaling factor and ΔE_0.

The validities of the scaled (model A) and unscaled (model B) fits may be compared by examining the self-consistency of the local thermochemical network of relative gas-phase acidities depicted in Figure 2. Internal inconsistencies in the relative acidities are obvious. For example, with model A the sum of $\Delta E_0(C_6H_5COOH, HNO_2) + \Delta E_0(HNO_2,HCOOH) = 16.9 \pm 5.0$ kJ/mol is not equal to the direct measurement $\Delta E_0(C_6H_5COOH,$-$HCOOH) = 26.0 \pm 4.2$ kJ/mol, but they must actually be equal. The internal discrepancies are even worse for model B, 8.2 ± 7.1 vs 22.2 ± 8.3 kJ/mol, respectively, for the same comparison. For the fits using the TS switching model for the higher-energy channel with an adjustable tight TS energy (not shown) the internal consistency is similarly poor, but the pattern of deviations is different. Clearly, something is wrong with one or more of the values. The self-consistency (or inconsistency)

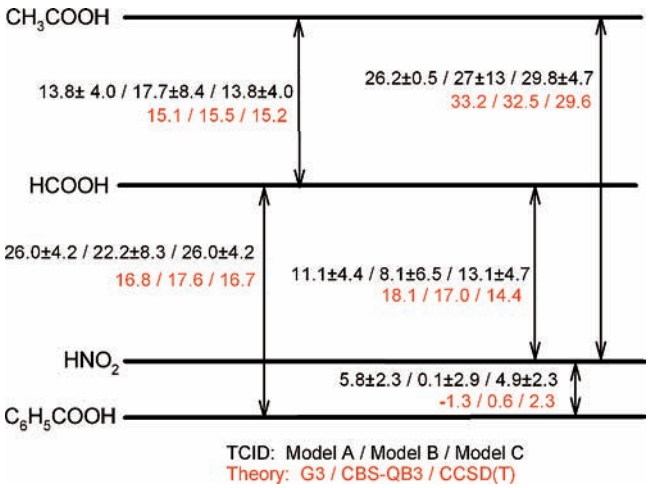

Figure 2. Local thermochemical network of relative gas-phase acidities in kJ/mol at 0 K. The values obtained by TCID models A, B, and C are shown on the first line (black) followed by those from G3, CBS-QB3, and CCSD(T) calculations (red).

of the thermochemical networks can be quantified using eq 6 as described previously.[2,4]

$$\chi_{\text{acid}}^{\,2} = \frac{\sum_{j\neq k}\left(\frac{\Delta_{\text{acid}}H_0(\text{HA}_j) - \Delta_{\text{acid}}H_0(\text{HA}_k) - \Delta E_0(j,k)}{\sigma_{j,k}}\right)^2}{\sum_{j\neq k}(1/\sigma_{j,k})^2} \quad (6)$$

The absolute gas-phase acidities are determined by a least-squares minimization of χ_{acid}^2, where $\Delta E_0(j,k)$ is the measured TCID threshold energy difference for the complex $[A_kHA_j]^-$, $\Delta_{\text{acid}}H_0(HA_j)$ and $\Delta_{\text{acid}}H_0(HA_k)$ are the absolute gas-phase acidities, and $\sigma_{j,k}$ is the uncertainty of the individual relative acidity measurement. The gas-phase acidity of nitrous acid,[26,27] $\Delta_{\text{acid}}H_0(HNO_2) = 1418.5 \pm 0.9$ kJ/mol (Table 2), is treated as the reference and the other acidities are obtained by minimization of χ_{acid}^2. The $\Delta E_0(j,k)$ values include 20 independent measurements of the five different complexes, with average values and the number of individual measurements for each complex listed in Table 1. The procedure for determining the uncertainties of the absolute gas-phase acidities has been described previously.[4] Table 2 gives the results for models A and B and compares them with literature experimental and theoretical values (described below). Comparison of the overall χ_{acid}^2 values and the uncertainties of the absolute acidities for the networks of these two models shows that the *unscaled* fits in model A provide a significantly more self-consistent set of relative acidities. That implies that using the extra adjustable parameter for one product channel is *not* justified even though the individual data fits are obviously improved. Nevertheless, the relatively poor fits for some of the reaction cross sections means that model A for the relative cross sections is not entirely accurate either. Furthermore, the internal consistency of the local thermochemical network with model A is poor compared with the networks we obtained in our previous TCID work on gas-phase acidities of alcohols.[2,4]

To check for experimental issues that could cause inconsistencies in the TCID results, the measurements were repeated several times under different source and ion focusing conditions and the ΔE_0 results were found to be reproducible. To check for possible mass overlap problems, the second stability region of the Mathieu equations was employed[7] in the quadrupole mass filter to achieve higher mass abundance sensitivity for $HCOO^-$ ($m/z = 45$), NO_2^- ($m/z = 46$) and their complexes. The initial magnetic sector mass spectrometer was also tuned to the low- or high-mass side of the peaks to check for possible mass overlaps between $HCOO^-$(HCOOH) and NO_2^-(HCOOH) complexes and in similar situations. These experiments found mass contamination effects to be negligible. Where possible, we tested different methods for forming the complex ions. For example, $[CH_3COO{\cdot}H{\cdot}OOCH]^-$ was produced both from CH_3COO^- + HCOOH and from $HCOO^-$ + CH_3COOH in the flow tube. The resulting TCID cross sections and threshold energies are the same within experimental uncertainties. Baring unidentified but reproducible reactant ion contaminants or excited states, we conclude that the inconsistencies in relative acidities are not due to instrumental or procedural artifacts and therefore we seek more fundamental explanations, which we defer to the Discussion section.

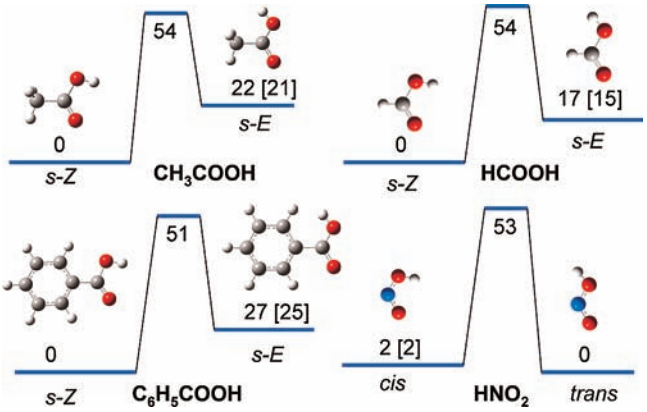

Figure 3. Isomers of HCOOH, CH_3COOH, HNO_2, and C_6H_5COOH with relative energies calculated at the B3LYP/aug-cc-pVDZ level without [and with] vibrational zero-point-energy corrections.

Computational Results

The relative energies of the *cis* and *trans* conformers of the four acids and their isomerization energies were calculated by density functional theory at the B3LYP/aug-cc-pVDZ level using Gaussian 03.[18−20] The structures and energies are shown in Figure 3. For simplicity and consistency in this work, we denote species with the HOCO or HONO dihedral angle near 0° as "*cis*" and those near 180° as "*trans*"; the *E*/*Z* designations are given in Figure 3. The transition states for isomerization between the two conformers were verified to have a single imaginary frequency. For the three carboxylic acids, the lower-energy conformation is *cis*, the *trans* conformer lies 15 to 25 kJ/mol higher, and the barrier heights are 51−54 kJ/mol. For nitrous acid, the *trans* conformer is 2 kJ/mol lower in energy than the *cis* conformer, which agrees well with the experimental value of 1.7 ± 0.4 kJ/mol,[28] and the calculated barrier height is 53 kJ/mol.

We also examined the structures of the proton-bound complexes **1** to **5** (Figure 4) at the B3LYP/aug-cc-pVDZ level. Starting with the ground-state conformers of the neutral acids, a hydrogen bond can be formed between the acid and one oxygen atom of a carboxylate or nitrite anion. However, formation of two hydrogen bonds or other favorable electrostatic interactions are possible if the acid isomerizes from the *cis* to *trans* conformation. The same is true if the other partner is treated as the acid and isomerizes, resulting in four major configurations of the complexes that we designate *cis*/*cis*, *cis*/*trans*, *trans*/*trans*, and *trans*/*cis* (larger species first). These

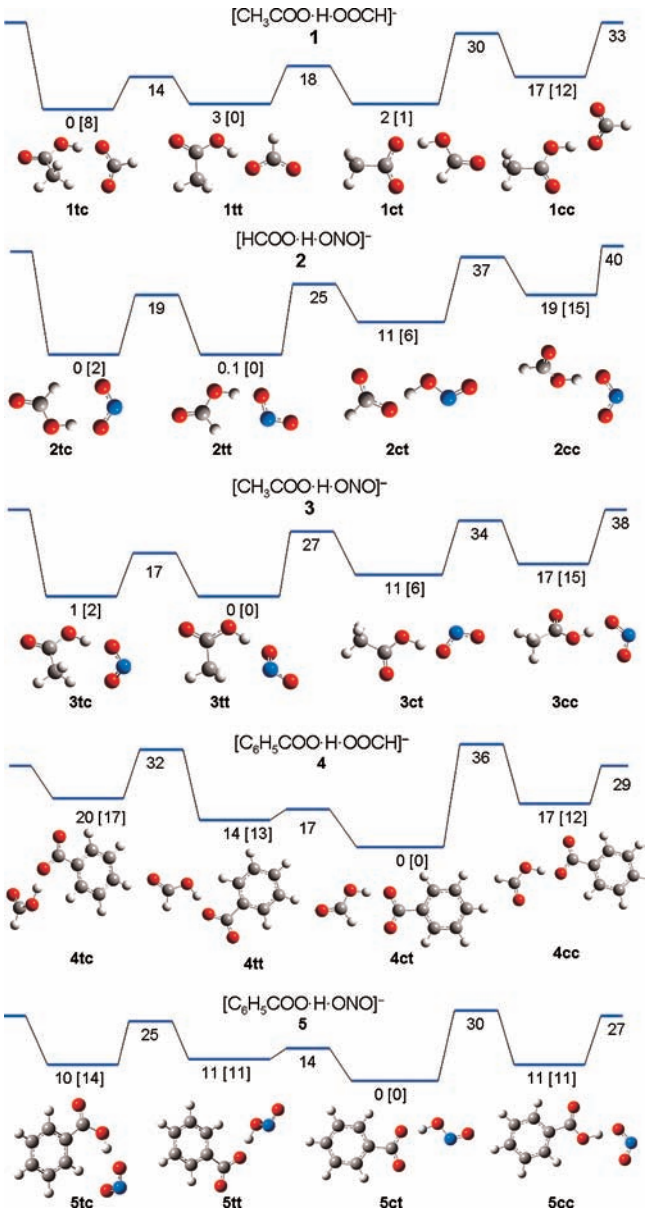

Figure 4. Energy levels and structures for conformations of the proton-bound cluster ions. The relative energies are calculated at the B3LYP/aug-cc-pVDZ level without [and with] vibrational zero-point-energy corrections.

structures and their relative energies are given in Figure 4 and Table 3. For four of the five complexes studied, the isomer formed from the ground-state conformations of both acids does *not* have the lowest energy. That is, the formation of a second hydrogen bond more than overcomes the isomerization energy of the free acid. The exception is the $C_6H_5COOH/\ NO_2^-$ cluster, whose *cis*/*trans* conform is lowest in energy and can dissociation without isomerization into ground-state products. To find the isomerization barrier energies, we scanned the HOCO or HONO dihedral angles by 5° increments in both possible directions, optimizing other degrees of freedom. These isomerization barriers, which range from 14 to 40 kJ/mol, are also shown in Figure 4.

The largest calculated barrier from a higher-energy complex conformation to a lower-energy conformation is 19 kJ/mol (**5cc** to **5ct** in Figure 4). That number is relevant for determining whether metastable isomers could be kinetically trapped in the flow tube reactor source. Using a simple Arrhenius model with a pre-exponential factor of 10^{13} s^{-1}, we estimate a isomer relaxation rate of 5×10^9 s^{-1} at room temperature for a barrier of 19 kJ/mol, which is much faster than both the collision frequency with the helium buffer gas of about 10^7 s^{-1} and the millisecond residence time in the flow tube. Therefore, we expect to have equilibrium concentrations of the proton-bound cluster ion conformations in the ion beam. The calculated equilibrium concentrations at the room temperature of the flow tube reactor are given in Table 3. Note that once the cluster ions leave the high-pressure region of the ion source, they undergo no collisions and cannot exchange energy until the single activating collision with the xenon target gas atom.

The 0 K gas-phase acidities of formic, acetic, benzoic, and nitrous acids were calculated by the Gaussian-3,[29] CBS-QB3,[30] and CCSD(T)[31] methods using Gaussian 03.[20] The results are listed in Table 2. The CCSD(T)/aug-cc-pVTZ single-point energy calculations and zero-point vibrational energy corrections are based on structures and harmonic frequencies from density functional theory at the B3LYP/aug-cc-pVTZ level.

For comparison, Table 2 also lists literature experimental thermochemical data for the three carboxylic acids, using $\Delta_{acid}G_{298}$ values from the NIST Webbook compilation.[32−35] These acidities are obtained by determining the equilibrium constants for the gas-phase reaction $A_1^- + HA_2 = HA_1 + A_2^-$, and thus should represent the acidity differences for ground-state species. We convert among $\Delta_{acid}H_0$, $\Delta_{acid}H_{298}$, and $\Delta_{acid}G_{298}$ using standard statistical mechanics formulas with the ro-vibrational parameters provided in the Supporting Information (Table S1). In one instance, our estimate of $\Delta_{acid}S_{298}$ differs significantly from the value used in the NIST compilation.[32] Specifically, our calculations show that CH_3COO^- has a nearly free rotation around the C−C bond, with six-fold symmetry and a barrier for the internal rotation less than 2 cm^{-1} at the B3LYP/aug-cc-pVDZ level, whereas previous evaluations of its thermodynamic functions[36,37] treated it as a harmonic vibration with a frequency of 204 cm^{-1}. Its treatment as a free rotor results in a lowering of $\Delta_{acid}H(CH_3COOH)$ by about 3 kJ/mol from the NIST value. The corrected experimental equilibrium results for $\Delta_{acid}H_0$ agree with our various theoretical calculations for the three carboxylic acids within 7 kJ/mol.

Discussion

The absolute gas-phase acidities derived from the TCID experiments are compared with the theoretical calculations and literature equilibrium experiments in Table 2. The acidities from the TCID fits from models A and B (described above) agree with the equilibrium and theoretical values within their uncertainties. However, that is not very meaningful because the internal inconsistencies of the local thermochemical network result in rather large experimental uncertainties. These uncertainties and deviations from theory are significantly greater than the errors found in our previous TCID measurements of alcohol acidities[2,4,6] Here we consider possible explanations for the TCID results on carboxylic acids.

One possible explanation for these discrepancies is that different tautomers of the anions are formed in the ion source. For example, an acetic acid molecule can lose a proton from the methyl group and form enolate, $^-CH_2COOH \leftrightarrow CH_2C(OH)O^-$, instead of carboxylate, CH_3COO^-. The enolate anion could combine with a formic acid molecule to form a doubly hydrogen-bonded complex, shown in Figure 5. However, at the B3LYP/aug-cc-pVDZ level this complex is 79 kJ/mol higher in energy than the lowest hydrogen-bonded complex in Figure 4, and its calculated dissociation energy is also much higher. Moreover, when $HCOO^-$ is used to combine with CH_3-

TABLE 3: Proton-Bound Cluster Ion Conformers, Calculated Relative Energies and Populations

	$[CH_3COO{\cdot}H{\cdot}OOCH]^-$ (**1**)			$[HCOO{\cdot}H{\cdot}ONO]^-$ (**2**)			$[CH_3COO{\cdot}H{\cdot}ONO]^-$ (**3**)			$[C_6H_5COO{\cdot}H{\cdot}OOCH]^-$ (**4**)			$[C_6H_5COO{\cdot}H{\cdot}ONO]^-$ (**5**)		
conformer[a]	δH_0[b]	δG_{298}[b]	pop.[c]	δH_0[b]	δG_{298}[b]	pop.[c]	δH_0[b]	δG_{298}[b]	pop.[c]	δH_0[b]	δG_{298}[b]	pop.[c]	δH_0[b]	δG_{298}[b]	pop.[c]
trans/cis	0.6	6.2	0.060	2.1	5.4	0.096	5.8	1.1	0.338	17.5	20.1	0.0003	13.9	19.1	0.0004
trans/trans	0.0	0.0	0.736	0.0	0.0	0.840	0.0	0.0	0.516	12.8	10.8	0.012	11.3	13.4	0.004
cis/trans	1.3	3.3	0.198	6.0	6.4	0.064	2.2	3.3	0.138	0.0	0.0	0.960	0.0	0.0	0.981
cis/cis	11.9	11.7	0.006	17.4	17.5	0.001	15.0	10.4	0.008	12.3	8.8	0.028	10.5	10.5	0.014

[a] Conformation refers to the HOCO or HONO dihedral angles (cis ≈ 0°, trans ≈ 180°), in the order of the acids as labeled in the first row, where H is the hydrogen-bonded proton. [b] Relative enthalpy at 0 K or Gibbs energy at 298 K calculated at the B3LYP/aug-cc-VDZ level, in kJ/mol, with vibrational energies in the harmonic oscillator approximation. [c] Relative equilibrium population at 298 K.

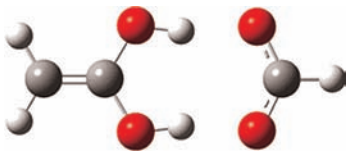

Figure 5. High-energy cluster ion isomer formed between CH_3COOH and $HCOO^-$.

COOH in the ion source, the complex in Figure 5 could not be produced directly because it requires the high-energy isomer $H_2C{=}C(OH)_2$ as the neutral. By similar considerations we can rule out the possibility that $HOCO^-$, instead of $HCOO^-$, combines with CH_3COOH. The gas-phase acidities associated with other deprotonation processes, i.e., $HCOOH \rightarrow HOCO^- + H^+$, $CH_3COOH \rightarrow {}^-CH_2COO + H^+$, and $C_6H_5COOH \rightarrow {}^-C_6H_4COOH + H^+$, are hundreds of kJ/mol higher in energy than deprotonation at the carboxylic group. Therefore, the involvement of enol tautomers can be excluded as the cause of the discrepancies.

Other possibilities for the thermochemical inconsistencies relate to the various conformations of the proton-bound cluster reactant ions (Figure 4) and of the product acids (Figure 3). These are not taken into account in models A and B (Tables 1 and 2). Because the detected ion has the same mass regardless of the neutral conformation, we cannot distinguish these product conformer channels experimentally. It is instructive to consider limiting cases. First, an extreme limit for the influence of the reactant and product conformations would be to consider the conformations of the two acids in proton-bound cluster ion to be locked in place with no isomerization allowed along the dissociation path. That would be the case if the barriers between the cluster structures were high relative to the dissociation energy. For example, in this "diabatic" limit the lowest-energy *trans/trans* conformer of $[HCOO{\cdot}H{\cdot}OOCCH_3]^-$ (**1**) could only dissociate into $HCOO^-$ + *trans*-CH_3COOH and CH_3COO^- + *trans*-HCOOH, both of which are excited product acid conformers. For four of the five reaction systems, the cluster ion with the largest equilibrium population from the ion source would *not* lead to the ground state for at least one channel in the diabatic limit. The Supporting Information includes diagrams showing these diabatic pathways for all five systems. To illustrate these effects, we have used CRUNCH to simulate the results for $[HCOO{\cdot}H{\cdot}OOCCH_3]^-$. Using the conformer energies from the B3LYP/aug-cc-pVDZ calculations, $\Delta E_0 = 0.158$ eV from CCSD(T)/aug-cc-pVTZ calculations, and typical values for other parameters, we calculated the cross sections for the four cluster ion conformations independently, then summed them weighted by the populations in Table 3. The *trans*/*trans* conformer of complex **1** contributes to both channels at energies well above threshold, whereas near threshold **1**(*trans*/*cis*) dominates for CH_3COO^- + HCOOH and **1**(*cis*/*trans*) dominates for $CH_3COOH + HCOO^-$. The other five pathways have much smaller relative cross sections, because of either high threshold energies or low initial population (for *cis*/*cis*), and do not significantly contribute. If we then treat the simulation as experimental data and fit it, we obtain $\Delta E_0 = 0.08$ eV using model A and $\Delta E_0 = 0.05$ eV using model B; i.e., both models yield large deviations from the value of ΔE_0 used to simulate the data. This result shows that strictly diabatic dissociation behavior would significantly affect the cross sections and apparent ΔE_0 values. The direction of the effect for each system will depend on the details of the relative conformer energies and populations. Given the heights of the isomerization barriers in Figure 4, however, it is unrealistic to say that the *trans*/*trans* isomer cannot access the ground-state *cis* product conformers at all.

A second limiting case would posit that all reactant ion conformations can dissociate statistically into all energetically accessible product conformer channels. This would be true for low isomerization barriers among the cluster ion conformations. To model this situation using RRKM theory (model C), we include (a) all four reactant conformations with Boltzmann populations using the relative energies given in Table 3 in the initial ion internal energy distribution, (b) the four reactant conformations in the calculation of the density of states $\rho(E)$ in eq 5, and (c) statistically independent product channels for both conformations of each neutral acid in the sum of states $N(E)$ in eq 5. For the sums and densities of states in the RRKM calculations, we use the good approximation that all conformations of a species have the same vibrational frequency distribution; i.e., they differ only by their energies. For the carboxylic acids, we use B3LYP/aug-cc-pVDZ for the product conformational isomerization energies; for nitrous acid we use the experimental value.[28] The quantitative results of model C are given in Tables 1 and 2; the fits to the data (not shown) are nearly indistinguishable from model A in Figure 1. We can evaluate each modification to model A as follows. (a) The inclusion of the reactant ion conformations in the internal energy distributions shifts the value of $E_0(1)$, but only by a few millielectronvolts corresponding to the mean populated energy at room temperature in the ion source. (b) The inclusion of the four conformations in $\rho(E)$ has virtually no effect on ΔE_0, because the density of states in the denominator of eq 5 cancels out in the ratio of rate constants in eq 4. (c) The inclusion of additional product conformer channels has no significant effect for the carboxylic acids because the higher-energy conformers lie 15−25 kJ/mol above the ground states. As a result, their relative formation rates are much smaller than those of the ground-state conformers; i.e., their contributions to the overall cross sections are 1−2 orders of magnitude smaller at high energies and much weaker near threshold. The primary effect of (c) is for the channels that form HNO_2, because the nearly isoenergetic *cis* and *trans* conformations of nitrous acid are statistically accessible. Indeed, nearly the same values of ΔE_0 as found in model C are obtained by simply doubling the reaction degeneracy (or scaling factor) for HNO_2 product channels and applying an energy correction for the *cis*/*trans*

energy difference. The self-consistency of the thermochemical network of relative acidities is improved for model C compared with model A (see χ_{acid}^2 in Table 2), resulting in somewhat smaller uncertainties in the absolute acidities of the carboxylic acids. The agreement of the absolute acidities with theory and equilibrium experiments is also better (Table 2), although the relative acidities of model C versus theory (Figure 2) still deviate significantly for the two clusters containing benzoic acid. The improvements imply that accounting for the HNO_2 conformations is important. The treatment of the two HNO_2 conformations as statistically independent product channels is certainly valid from threshold up to the 53 kJ/mol isomerization barrier, and is a reasonable approximation above the barrier because each conformer supports nearly harmonic vibrational modes. We therefore consider model C to provide the "best" TCID results within the statistical RRKM theory framework. The use of multiple interlocking relative acidities measurements in the local thermochemical network forces reasonable absolute acidities with properly estimated uncertainties. That is a great advantage of this procedure. However, the final uncertainties for the absolute acidities of 4−6 kJ/mol (0.04−0.06 eV) for model C in Table 2 are *larger* than the experimental uncertainties of the individual ΔE_0 measurements in Table 1. Usually the goal is to *reduce* the uncertainties by application of eq 6 on multiple interlocking relative acidity measurements. The remaining deviations suggest that the statistical model is still not a completely accurate representation of the TCID process for all of these systems.

The calculated barriers between the reactant ion conformational structures range up to about 40% of the dissociation energies, so neither the completely diabatic nor the completely statistical limits discussed above may apply exactly. To understand how these barriers might affect the statistical dissociation kinetics, consider the simplified potential energy surface in Figure 6. This shows the dissociation of a cluster ion to one product channel via a direct barrierless pathway, and reaching the other product channel requires passage over an intermediate barrier through a different cluster conformation. Figure 6 also shows simulated cross sections for the two product channels as a function of the height of the intermediate barrier. For these simulations, we use the transition-state-switching model with a tight transition state (cluster frequencies with a low-frequency mode removed as the isomerization reaction coordinate) at the intermediate barrier. The frequencies are taken from the $[HCOO{\cdot}H{\cdot}OOCCH_3]^-$ system. These simulations demonstrate that the product branching ratio above threshold is a sensitive function of the height of the intermediate barrier. That is, if the cluster ion conformation populated in the ion beam must pass over an isomerization barrier to form the ground-state product acid conformer, its dissociation rate can be diminished relative to a direct dissociation with a simple loose transition state. That changes the product branching ratio in eq 4 and therefore affects the competitive shifts between the two product ions. As a result, the ΔE_0 value obtained with fits using a loose TS model would change to compensate. Fundamentally, this can at least partially explain why the loose TS models fit the data best only near threshold and the deviations in relative acidities. One could in principle attempt to fit the data using the transition-state-switching models for the dissociation pathways where isomerization is required to reach ground-state products. However, that would introduce several additional model parameters (barrier heights for multiple conformational pathways), which are not justified statistically in the least-squares fits given that we only measure the cross sections.

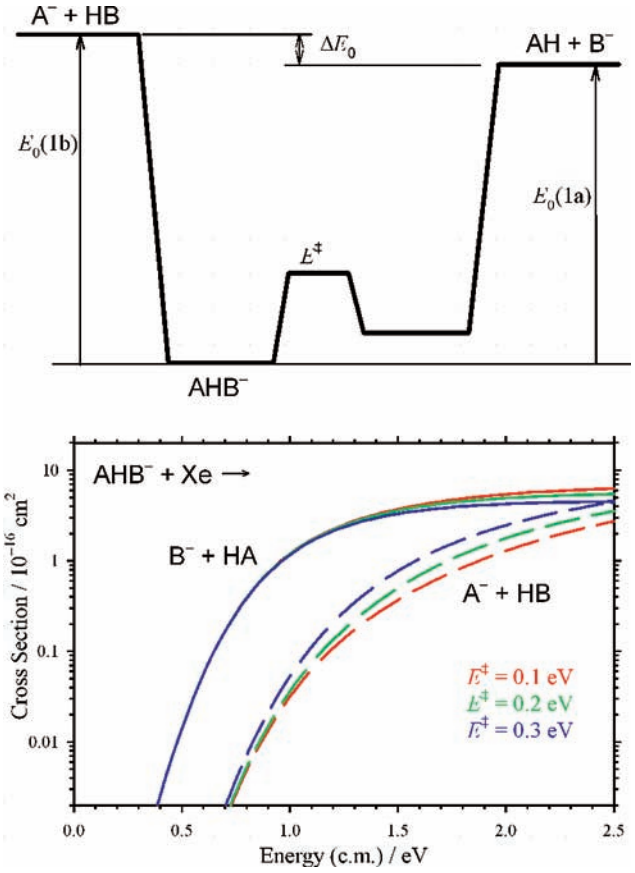

Figure 6. Simulation of the competition between dissociations of a complex AHB^- that can occur via a direct barrierless pathway to (1a) $A^- + HB$ or by passing over an intermediate isomerization barrier to (1b) $B^- + HA$, as shown in the schematic energy level diagram (top). The simulated cross sections use a loose orbiting transition state for channel 1a (solid lines) and a transition-state-switching model for channel 1b (dashed lines) with $E_0(1a) = 1.0$ eV and $\Delta E_0 = 0.1$ eV. For the transition-state-switching model the height of the intermediate barrier is $E^‡ = 0.1$ eV (red lines), $E^‡ = 0.2$ eV (green lines), or $E^‡ = 0.3$ eV (blue lines).

As an aside we note that, according to the Curtin−Hammet principle[38] for a reaction system in thermal equilibrium, the equilibrium concentration of two reactant isomers in fast pre-equilibrium does not affect the relative formation rates of two slower product channels associated separately with the two isomers. The Curtin−Hammet principle does not apply, however, to the present nonequilibrium system in which the reactant molecules are isolated gas-phase ions. For instance, if a higher-energy ion conformation emerges from the source, it necessarily retains the extra internal energy and can therefore exhibit different dissociation kinetics behavior than the predominant low-energy conformation, regardless of whether the isomerization barriers are high enough to trap it in a single conformational structure.

Finally, let us consider how the isomerization barrier heights change dynamically as the cluster ion dissociates. The calculated barriers for isomerization of the cluster ions are well below the total energy after the activating collision. However, as the cluster pulls apart the isomerization barrier increases toward the value for the free acids and the cluster's internal vibrational energy is converted into potential energy of the ion/molecule pair. Therefore, at some point along the dissociation reaction path the product acid is "locked" into one conformation. For total energies near the threshold, the point of locking is fairly early in the dissociation process. In this situation, which likely applies

to the present systems, the dissociation process may either be partly nonstatistical or else require a sophisticated variable transition-state model that accounts for the multiconfigurational potential energy surface. Given our limited knowledge of the complex potential energy surfaces including all the degrees of freedom in these large systems, a full dynamic treatment (e.g., trajectory calculations) or a full variable transition-state theory is not practical and is beyond the scope of this work. However, such dynamic effects are a plausible explanation for the deviations of the relative acidities found in these systems by the TCID method.

Conclusions

We have investigated the threshold collision-induced dissociation processes of the hydrogen-bonded dimers $[CH_3COO{\cdot}H{\cdot}OOCH]^-$, $[CH_3COO{\cdot}H{\cdot}ONO]^-$, $[HCOO{\cdot}H{\cdot}ONO]^-$, $[C_6H_5COO{\cdot}H{\cdot}OOCH]^-$, and $[C_6H_5COO{\cdot}H{\cdot}ONO]^-$. The reaction cross sections and branching ratios were modeled by RRKM theory, and the relative activation energies for dissociation were found. If these relative energies are ascribed to thermochemical acidity differences, there arise significant internal inconsistencies in the relative acidities. These deviations are most likely caused by formation of conformational structures of the proton-bound complexes that must isomerize along the dissociation pathway to reach ground-state product conformers. The isomerization barriers, although below the total available energy, can affect the kinetics of dissociation to ground-state products and therefore affect the branching ratios between the two proton-transfer channels. The most significant deviations in relative acidities between the best statistical treatment (model C) and theory is for the systems containing benzoic acid (see Figure 2). We have no definitive explanation as to why these systems might be unique, but they are the largest clusters (which increases the dissociative lifetime and might amplify competitive shift effects) and have *cis*/*trans* ground-state isomers versus *trans*/*trans* or *trans*/*cis* for the other three systems (Figure 4). The reaction dynamics of dissociation from multiple cluster ion conformations into multiple conformations of the products is complicated and are beyond the scope of the RRKM models employed here. Trajectory dynamics calculations might be able to address these issues.

Despite the internal inconsistencies in individual relative acidity measurements by TCID, the use of a local thermochemical network with multiple redundant and interconnected relative acidity measurements constrains the absolute acidities to values that agree reasonably with theory and previous equilibrium measurements within their uncertainties. That is fortunate but conversely means that acidity (or other ion affinity) thermokinetic measurements using a single unknown/reference pair are suspect when multiple conformations or binding sites are involved. Thus, thermokinetic dissociation methods are not optimal for systems where interactions within the complex can induce conformational changes. This conclusion may have serious implications, for example, for acidity determinations of amino acids by thermokinetic methods that employ dissociation of a proton-bound heterodimer.[39,40] In recent work, Bouchoux used the kinetic method to determine the proton affinities of a series of bidentate molecules and found the values differ from those obtained by equilibrium method in the case of diols.[41] That result is likely also due complications from multiple hydrogen bonding interactions. Both the competitive TCID method used here and the Cooks kinetic method[42,43] are based on the assumptions that there are no reverse activation energies for the dissociations and that the molecules are not involved in any isomerization processes. A most serious problem in application of these thermokinetic methods arises when, as stated by Cooks, "the cluster ion does not have the structure assigned to it ... for example, when there are multiple binding sites in a molecule".[43]

Acknowledgment. This research is funded by the U.S. Department of Energy, Office of Science, Office of Basic Energy Sciences, Chemical Sciences, Geosciences, and Biosciences Division.

Supporting Information Available: Rotational constants and vibrational frequencies used in the RRKM models and for the thermal corrections are listed in Table S1. The calculated structures of the cluster ion isomers are presented in Table S2−S9. The structures of the neutral acid molecules and their conjugate bases are given in Table S10−S21. Diagrams showing dissociation pathways between the cluster ion and product conformations are shown in Figures S1−S5. This material is available free of charge via the Internet at http://pubs.acs.org.

References and Notes

(1) Rodgers, M. T.; Armentrout, P. B. *J. Chem. Phys.* **1998**, *109*, 1787.
(2) DeTuri, V. F.; Ervin, K. M. *J. Phys. Chem. A* **1999**, *103*, 6911.
(3) Angel, L. A.; Ervin, K. M. *J. Phys. Chem. A* **2004**, *108*, 8345.
(4) Angel, L. A.; Ervin, K. M. *J. Phys. Chem. A* **2006**, *110*, 10392.
(5) Rodgers, M. T.; Ervin, K. M.; Armentrout, P. B. *J. Chem. Phys.* **1997**, *106*, 4499.
(6) Ervin, K. M.; DeTuri, V. F. *J. Phys. Chem. A* **2002**, *106*, 9947.
(7) DeTuri, V. F.; Hintz, P. A.; Ervin, K. M. *J. Phys. Chem. A* **1997**, *101*, 5969.
(8) *Dictionary of Inorganic Compounds*; Macintyre, J. E., Ed.; Chapman & Hall: London 1992; Vol. 3, p 3331.
(9) Gerlich, D. *Adv. Chem. Phys.* **1992**, *82*, 1.
(10) Ervin, K. M.; Armentrout, P. B. *J. Chem. Phys.* **1985**, *83*, 166.
(11) Muntean, F.; Armentrout, P. B. *J. Chem. Phys.* **2001**, *115*, 1213.
(12) Baer, T.; Hase, W. L. *Unimolecular Reaction Dynamics: Theory and Experiments*; Oxford University Press: New York 1996.
(13) Gilbert, R. G.; Smith, S. C. *Theory of Unimolecular and Recombination Reactions*; Blackwell Scientific: Boston 1990.
(14) Beyer, T. S.; Swinehart, D. F. *Commun. ACM* **1973**, *16*, 379.
(15) Stein, S. E.; Rabinovitch, B. S. *J. Chem. Phys.* **1973**, *58*, 2438.
(16) Stein, S. E.; Rabinovitch, B. S. *Chem. Phys. Lett.* **1977**, *49*, 183.
(17) Chesnavich, W. J.; Bass, L.; Su, T.; Bowers, M. T. *J. Chem. Phys.* **1981**, *74*, 2228.
(18) Lee, C.; Yang, W.; Parr, R. G. *Phys. Rev. B* **1988**, *37*, 785.
(19) Dunning, T. H., Jr. *J. Chem. Phys.* **1989**, *90*, 1007.
(20) Frisch, M. J.; Trucks, G. W.; Schlegel, H. B.; Scuseria, G. E.; Robb, M. A.; Cheeseman, J. R.; Montgomery, J. A., Jr.; Vreven, T.; Kudin, K. N.; Burant, J. C.; Millam, J. M.; Iyengar, S. S.; Tomasi, J.; Barone, V.; Mennucci, B.; Cossi, M.; Scalmani, G.; Rega, N.; Petersson, G. A.; Nakatsuji, H.; Hada, M.; Ehara, M.; Toyota, K.; Fukuda, R.; Hasegawa, J.; Ishida, M.; Nakajima, T.; Honda, Y.; Kitao, O.; Nakai, H.; Klene, M.; Li, X.; Knox, J. E.; Hratchian, H. P.; Cross, J. B.; Bakken, V.; Adamo, C.; Jaramillo, J.; Gomperts, R.; Stratmann, R. E.; Yazyev, O.; Austin, A. J.; Cammi, R.; Pomelli, C.; Ochterski, J. W.; Ayala, P. Y.; Morokuma, K.; Voth, G. A.; Salvador, P.; Dannenberg, J. J.; Zakrzewski, V. G.; Dapprich, S.; Daniels, A. D.; Strain, M. C.; Farkas, O.; Malick, D. K.; Rabuck, A. D.; Raghavachari, K.; Foresman, J. B.; Ortiz, J. V.; Cui, Q.; Baboul, A. G.; Clifford, S.; Cioslowski, J.; Stefanov, B. B.; Liu, G.; Liashenko, A.; Piskorz, P.; Komaromi, I.; Martin, R. L.; Fox, D. J.; Keith, T.; Al-Laham, M. A.; Peng, C. Y.; Nanayakkara, A.; Challacombe, M.; Gill, P. M. W.; Johnson, B.; Chen, W.; Wong, M. W.; Gonzalez, C.; Pople, J. A. *Gaussian 03*, revision C.02; Gaussian, Inc.: Wallingford, CT, 2004.
(21) Lifshitz, C.; Wu, R.; Tiernan, T. O.; Terwilleger, D. T. *J. Chem. Phys.* **1978**, *68*, 247.
(22) Armentrout, P. B.; Ervin, K. M. CRUNCH, Fortran program, version 5.1; University of Utah and University of Nevada: Salt Lake City and Reno, 2007.
(23) Muntean, F.; Armentrout, P. B. *J. Phys. Chem. A* **2003**, *107*, 7413.
(24) Narancic, S.; Bach, A.; Chen, P. *J. Phys. Chem. A* **2007**, *111*, 7006.
(25) Taylor, B. N.; Kuyatt, C. Guidelines for Evaluating and Expressing the Uncertainty of NIST Measurement Results; NIST Technical Note 1297; National Institute of Standards and Technology: Washington DC, 1994.
(26) Gurvich, L. V.; Veyts, I. V.; Alcock, C. B. *Thermodynamic Properties of Individual Substances*, 4th ed.; Elements O, H (D, T), F, Cl,

Br, I, He, Ne, Ar, Kr, Xe, Rn, S, N, P and Their Compounds; Hemisphere Publishing Corp.: New York, 1989; Vol. 1, Parts 1 and 2.

(27) Ervin, K. M.; Ho, J.; Lineberger, W. C. *J. Phys. Chem.* **1988**, *92*, 5405.

(28) Varma, R.; Curl, R. F. *J. Phys. Chem.* **1976**, *80*, 402.

(29) Curtiss, L. A.; Raghavachari, K.; Redfern, P. C.; Rassolov, V.; Pople, J. A. *J. Chem. Phys.* **1998**, *109*, 7764.

(30) Montgomery, J. A., Jr.; Frisch, M. J.; Ochterski, J. W.; Petersson, G. A. *J. Chem. Phys.* **1999**, *110*, 2822.

(31) Pople, J. A.; Head-Gordon, M.; Raghavachari, K. *J. Chem. Phys.* **1987**, *87*, 5968.

(32) Bartmess, J. E. Negative Ion Energetics Data, In *NIST Chemistry WebBook, NIST Standard Reference Database Number 69*; Mallard, W. G.; Linstrom, P. J., Eds.; National Institute of Standards and Technology: Gaithersburg, MD, June 2005. (http://webbook.nist.gov/chemistry/).

(33) Fujio, M.; McIver, R. T., Jr.; Taft, R. W. *J. Am. Chem. Soc.* **1981**, *103*, 4017.

(34) Taft, R.; Topsom, R. *Prog. Phys. Org. Chem.* **1987**, *16*, 1.

(35) Caldwell, G.; Renneboog, R.; Kebarle, P. *Can. J. Chem* **1989**, *67*, 661.

(36) Loewenschuss, A.; Marcus, Y. *Chem. Rev.* **1984**, *84*, 89.

(37) Loewenschuss, A.; Marcus, Y. *J. Phys. Chem. Ref. Data* **1987**, *16*, 61.

(38) Seeman, J. I. *Chem. Rev.* **1983**, *83*, 84.

(39) O'Hair, R. A. J.; Bowie, J. H.; Gronert, S. *Int. J. Mass Spectrom. Ion Processes* **1992**, *117*, 23.

(40) Tian, Z.; Pawlow, A.; Poutsma, J. C.; Kass, S. R. *J. Am. Chem. Soc.* **2007**, *129*, 5403.

(41) Bouchoux, G.; Buisson, D.-A.; Bourcier, S.; Sablier, M. *Int. J. Mass Spectrom.* **2003**, *228*, 1035.

(42) Cooks, R. G.; Koskinen, J. T.; Thomas, P. D. *J. Mass Spectrom.* **1999**, *34*, 85.

(43) Cooks, R. G.; Wong, P. S. H. *Acc. Chem. Res.* **1998**, *31*, 379.